

## A global empirical model for estimating zenith tropospheric delay

YAO YiBin<sup>1,2\*</sup>, ZHANG Bao<sup>1</sup>, XU ChaoQian<sup>1</sup>, HE ChangYong<sup>1</sup>, YU Chen<sup>1</sup> & YAN Feng<sup>1</sup>

<sup>1</sup> School of Geodesy and Geomatics, Wuhan University, Wuhan 430079, China;

<sup>2</sup> Key Laboratory of Geospace Environment and Geodesy, Ministry of Education, Wuhan 430079, China

Received April 2, 2015; accepted July 20, 2015; published online August 31, 2015

**Abstract** Tropospheric delay acts as a systematic error source in the Global Navigation Satellite Systems (GNSS) positioning. Empirical models UNB3, UNB3m, UNB4 and EGNOS have been developed for use in Satellite-Based Augmentation Systems (SBAS). Model performance, however, is limited due to the low spatial resolution of the look-up tables for meteorological parameters. A new design has been established in this study for improving performance of the tropospheric delay model by more effectively eliminating the error produced by tropospheric delay. The spatiotemporal characteristics of the Zenith Tropospheric Delay (ZTD) were analyzed with findings that ZTD exhibits different annual variations at different locations and decreases exponentially with height increasing. Spherical harmonics are utilized based on the findings to fit the annual mean and amplitude of the ZTD on a global scale and the exponential function is utilized for height corrections, yielding the ZTrop model. On a global scale, the ZTrop features an average deviation of  $-1.0$  cm and Root Mean Square (RMS) of  $4.7$  cm compared with the International GNSS Service (IGS) ZTD products, an average deviation of  $0.0$  cm and RMS of  $4.5$  cm compared with the Global Geodetic Observing System (GGOS) ZTD data, and an average deviation of  $-1.3$  cm and RMS of  $5.2$  cm compared with the ZTD data from the Constellation Observing System of Meteorology, Ionosphere, and Climate (COSMIC). The RMS of the ZTrop model is  $14.5\%$  smaller than that of UNB3,  $6.0\%$  smaller than that of UNB3m,  $16\%$  smaller than that of UNB4,  $14.5\%$  smaller than that of EGNOS and equivalent to the sophisticated GPT2+Saas model in comparison with the IGS ZTD products. The ZTrop, UNB3m and GPT2+Saas models are finally evaluated in GPS-based Precise Point Positioning (PPP), as the models act to aid in obtaining PPP position error less than  $1.5$  cm in north and east components and relative large error ( $>5$  cm) in up component with respect to the random walk approach.

**Keywords** Zenith tropospheric delay, Spherical harmonics, Exponential function, ZTrop model

**Citation:** Yao Y B, Zhang B, Xu C Q, He C Y, Yu C, Yan F. 2016. A global empirical model for estimating zenith tropospheric delay. Sci China Earth Sci, 59: 118–128, doi: 10.1007/s11430-015-5173-8

### 1. Introduction

Radio signals undergo two effects when passing through a neutral atmosphere, i.e. time delay and bending, resulting in signal propagation refraction, commonly known as propagation delay. In the Global Navigation Satellite Systems (GNSS), this delay is referred to as tropospheric delay and can be over  $2$  m at the zenith and over  $20$  m at the lower

receiver-to-satellite angles as the mapping function value is approximately  $10$  at elevation angle of  $\sim 5^\circ$  (Penna et al., 2001). Tropospheric delay on GNSS signals is amongst main error sources affecting positioning accuracy. Though larger than the tropospheric delay, ionospheric delay acts dispersively and closely related to frequency of the signal, thus eliminating the first-order effect by combinations of radio signals differing in frequency. Tropospheric delay does not depend on the frequency, thus may not be eliminated in a similar way. The tropospheric delay is either predicted by models or estimated as unknown parameters in

\*Corresponding author (email: ybyao@whu.edu.cn)

satellite positioning.

Conventional tropospheric delay models such as the Hopfield model (Hopfield, 1971) and the Saastamoinen model (Saastamoinen, 1972) may achieve centimeter-level accuracy when applying accurate *in-situ* meteorological observations. Janes et al. (1991) utilized ray-tracing solutions to examine accuracy of several models for tropospheric delay prediction and recommended the explicit form of the Saastamoinen zenith delay expressions. Comparing the models for tropospheric zenith delay against ray-tracing utilizing radiosonde profiles, Mendes and Langley (1999) concluded that zenith hydrostatic delay (ZHD) may be predicted with submillimetre accuracy utilizing accurate measurements of station pressure, while the zenith wet delay (ZWD) typically may be predicted with a precision of ~3 cm utilizing meteorological data due to high temporal and spatial variability. If *in-situ* meteorological observations are replaced by empirical values, the accuracy of these models will decline (Li et al., 2012). Since a large number of GNSS stations presently lack meteorological measurement equipment, the conventional tropospheric delay models are of limited use.

Collins and Langley (1997) proposed the UNB3 model for the Wide Area Augmentation System (WAAS) users across North America. The UNB3 model is based on prediction of meteorological parameter values, then applied to compute hydrostatic and non-hydrostatic delays utilizing the Saastamoinen model and Neill mapping functions (Collins et al., 1998). Seasonal variations of troposphere behavior are accounted for by utilizing a look-up table with annual mean and amplitude for temperature, pressure, water vapor pressure, temperature lapse rate and water vapor lapse rate varying with respect to latitude and height. Applied in several regions of the world, the UNB3 model may predict ZTD with a mean bias of 2.0 cm and a mean RMS of 5.2 cm under normal atmospheric conditions (Leandro et al., 2006). Relative humidity computed from predicted water vapor pressure values, however, was found to be potentially greater than 100%, which is not realistic (Leandro et al., 2006). A new version referred to as UNB3m, was then developed as a solution, with the water vapor pressure replaced by relative humidity in the UNB3m look-up table. The UNB3m demonstrated an improvement in bias (the average is -0.5 cm), and a mean RMS of 4.8 cm (Leandro et al., 2006). Collins et al. (1996) proposed that variation in temperature profiles significantly impact determination of ZHD, and modified the temperature and the temperature lapse rate parameters and utilized a constant temperature lapse rate of 6.5 K/km above the tropospheric boundary to maintain a certain consistency at all heights. The changes applied to UNB3 created the UNB4 model and operated to improve performance of UNB3 at low latitudes with a much lower bias, yet the two models exhibited the same standard deviation (~5 cm) (Collins et al., 1996). The European Geo-stationary Navigation Overlay System (EGNOS) guidelines recommend that a user applies a correction for

tropospheric delay that is compliant with the International Civil Aviation Organisation (ICAO) Standards and Recommended Practices for SBAS. These guidelines also cover the USA WAAS and the Japanese Multi-functional Transport Satellite, MTSAT-based Satellite Augmentation System (Penna et al., 2001). The tropospheric delay model (hereafter referred to as the EGNOS model) recommended by SBAS utilizes the same look-up table as UNB3 to provide empirical meteorological parameters utilized to calculate the ZTD by simplified equations (Tuchband, 2010). The RMS errors of the EGNOS model ranged from 4.0 to 4.7 cm (Penna et al., 2001) for five stations in the UK. The four models are based on a look-up table for five empirical meteorological parameters, thus the accuracy of these parameters significantly affects the accuracy of the models. Changes in temperature exert significant impact on ZHD at low altitudes while changes in water vapor pressure exert great impact on ZWD (Collins et al., 1996). Spatial resolution of the look-up tables are too limited for accuracy as annual mean and amplitude of the meteorological parameters are provided every 15° latitude from 15°N to 75°N and differences of meteorological variables between longitudes are ignored. Meteorological parameters obtained by interpolation from the look-up tables then can hardly be accurate. Different from UNB models in modeling principles, Li et al. (2012) developed a new ZTD correction model named IGGtrop, with a mean bias of -0.8 cm and a mean RMS of 4.0 cm with respect to GNSS-derived ZTD values from 125 global IGS sites. The IGGtrop features a relatively high accuracy; however, too many parameters render it complicated to use as it provides annual mean and amplitude of ZTD at a very high spatial resolution of 2.5°×2.5°×1 km. Later in 2015, Li et al. (2015) published the new versions of the IGGtrop model that reduced the number of parameters and also optimized storage. Disadvantages in UNBs, EGNOS and IGGtrop incentivize the goal to develop a better, appropriate and globally applicable ZTD model. Adopting the idea in weighted mean temperature model (Yao et al., 2013), a direct connection between day of the year (doy) and ZTD was established by first calculating annual mean and amplitude of ZTD at 5°×4° (lon×lat) grid points. Spherical harmonics are then utilized to fit annual mean and amplitude respectively, reducing model parameters and avoiding the interpolation. Validated by IGS ZTD products, COSMIC-derived ZTD and VMF1 (Boehm et al., 2006) ZTD, the new model (called ZTrop) demonstrates a higher accuracy than the UNB and EGNOS models, achieving the original goal. As Tuchband (2010) evaluated the EGNOS model in PPP, the ZTrop model is applied in PPP and applicability of the ZTrop model in GPS positioning is discussed.

## 2. Data sets

GGOS Atmosphere (<http://ggosatm.hg.tuwien.ac.at/>) is de-

signed to establish atmospheric models. The GGOS Atmosphere provides gridded VMF1 coefficients (Boehm et al., 2006) on a global grid with  $2.5^\circ \times 2^\circ$  (lon×lat) sampling at 00:00, 06:00, 12:00 and 18:00 UTC per day (<http://ggosatm.hg.tuwien.ac.at/DELAY/GRID/STD>). In addition to VMF1 coefficients, the ZHDs and ZWDs are also provided on the grid and calculated from reanalysis data provided by the European Centre for Medium-Range Weather Forecasts (ECMWF). ZTD is derived by adding the ZHD and the ZWD of the same place and time. The GGOS ZTD data from January 1st, 2008 to December 31st, 2011 are utilized to establish the new model and data in the whole 2012 are applied to validate the new model.

ZTD corrections at the International GNSS Service (IGS) stations are estimated by IGS associate analysis centers in support of the IGS Troposphere Working Group and may be located in subdirectories within the weekly GPS product directories (<ftp://cddis.gsfc.nasa.gov/pub/gps/products/WWW/trop>, where WWW equals the GPS week number). ZTDs are calculated by Gipsy-Oasis software (Webb, 1993) utilizing IGS orbit and clock products and site RINEX files. ZTDs are provided every 5 minutes with an accuracy of roughly 4 mm (Wang et al., 2007). IGS ZTD data at 123 stations in the whole 2010 are utilized to validate the new model.

COSMIC (Constellation Observing System of Meteorology, Ionosphere, and Climate) is a project set with space science experiments for detecting the atmosphere, customized by the US Department of Defense and Taiwan area at the end of the last century. Meteorological profiles may be acquired from COSMIC's website (<http://cosmicio.cosmic.ucar.edu/cdaac>) containing 400 layers of temperature, pressure, and water vapor pressure profiles with vertical resolution 100 m. Profiles may then be applied to calculate the atmospheric refractivity which may be expressed as:

$$N = k_1 \frac{P}{T} + k_2' \frac{P_v}{T} + k_3 \frac{P_v}{T^2}, \quad (1)$$

where  $N$  is the atmospheric refractivity,  $P$  is the pressure,  $T$  is the temperature,  $P_v$  is the vapor pressure, the  $k_1$ ,  $k_2'$  and  $k_3$  are the atmospheric refractivity constants (Davis et al., 1985; Bevis et al., 1994). The atmospheric refractivity may be utilized along the zenith direction to compute the integral for ZTD by:

$$ZTD = \int_s 10^{-6} N dh. \quad (2)$$

The GGOS ZTDs are provided at the global  $2.5^\circ \times 2^\circ$  (lon×lat) grid points with a strict schedule, thus are suitable for the new model's establishment and validation. As the IGS stations are sparsely scattered on the globe and the COSMIC occultations are irregularly scattered on earth, these two data types are not suitable for modeling application and are applied only to validate the new model in this

study. Figure 1 illustrates distributions of the global COSMIC occultations on January 1 and January 2, 2010, demonstrating that radio occultation observations have no repeatability in location.

### 3. Spatial and temporal characteristics of ZTD

Meteorological variables generally present annual periodic variations as well as regional differences. Eqs. (1) and (2) demonstrate that ZTD is determined by meteorological variables, so the ZTD is very likely to have some periodic characters like the meteorological variables.

Figure 2 describes the ZTD (data from GGOS Atmosphere) variations with time in 7 representative regions. As ZTD is mainly affected by latitudes on the surface of the Earth, the 7 regions represent upper-, middle- and low-latitudes of the southern and northern hemispheres, respectively.

As observed from Figure 2 and from Li et al. (2012), the ZTD in several areas presents a periodical change with an approximate 1-year cycle. ZTD is a function of meteorological variables which typically change in an annual cycle allowing ZTD to be expressed as a function of *doy* utilizing a cosine function as follows:

$$ZTD(doy) = \alpha_1 + \alpha_2 \times \cos(2\pi(doy - 28)/365.25), \quad (3)$$

where  $\alpha_1$  is the annual mean of ZTD,  $\alpha_2$  is the amplitude of ZTD, and the phase offset is fixed to January 28 (Boehm et al., 2007; Niell, 1996).

The ZTD substantially varied with latitude, as known, with magnitude appearing larger at low latitudes, smaller at high latitudes and asymmetric between the southern and northern hemispheres. Longitude also exerts influence on ZTD as various topography at locations with the same latitude but different longitudes creates significantly different meteorological values. The weather in Lop Nur in summer is extremely dry and hot, for instance, while at the same latitude, in Japan, the weather is very wet and cool. An accurate ZTD empirical model then requires both the latitude and longitude differences to be considered.

The ZHD can be seen as a function of pressure (Saast-

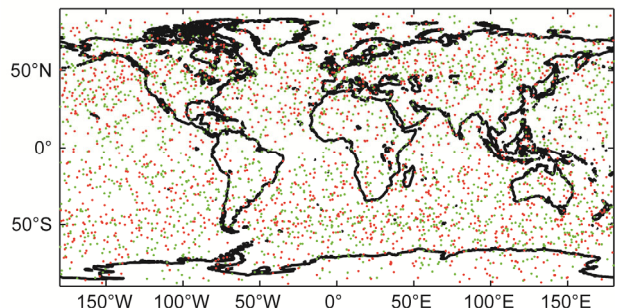


**Figure 1** Global distribution of COSMIC occultations on January 1 (green points) and January 2 (red points), 2010.

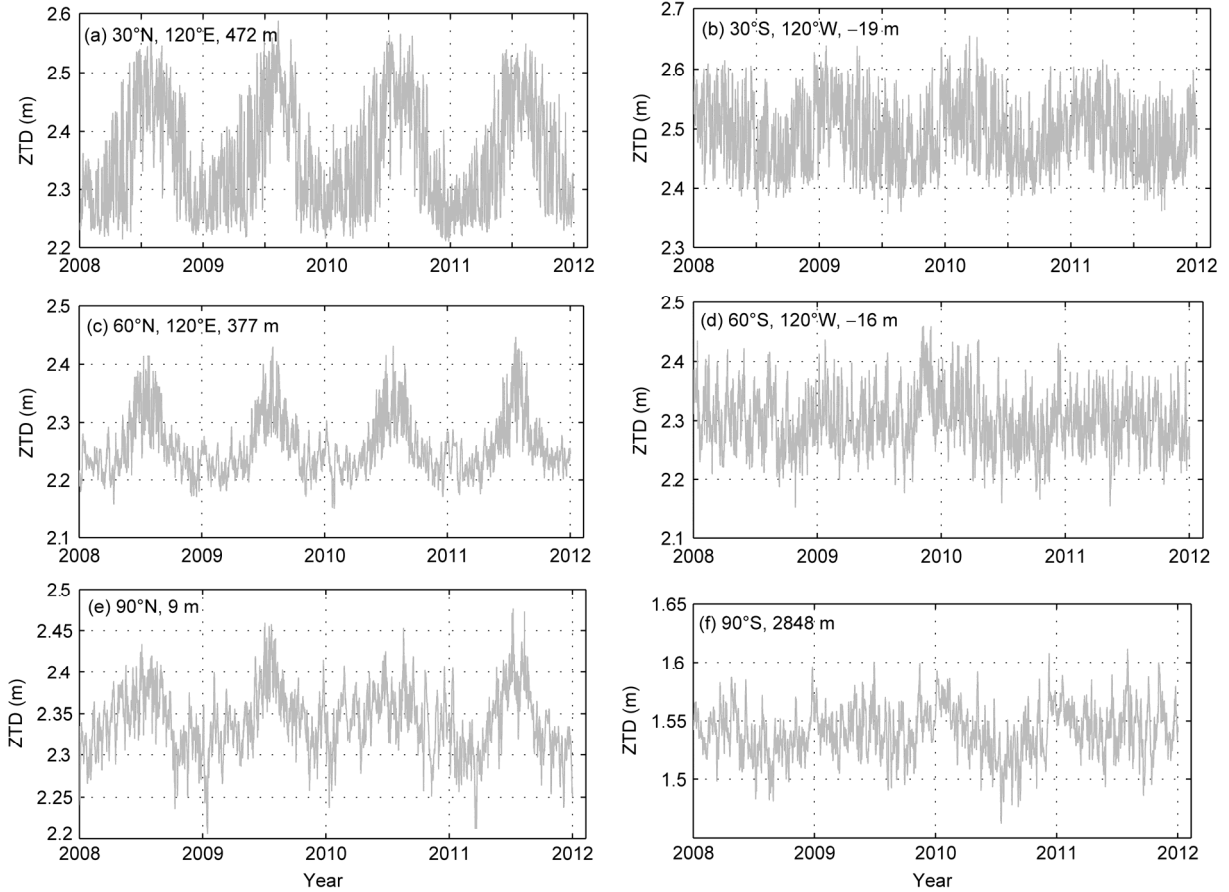


**Figure 2** ZTD time series from 2008 to 2011 at upper-, middle-, and low-latitudes and ellipsoidal heights. (a) 30°N, 120°E, 472 m; (b) 30°S, 120°W, -19 m; (c) 60°N, 120°E, 377 m; (d) 60°S, 120°W, -16 m; (e) 90°N, 9 m; (f) 90°S, 2848 m.

amoinen, 1972) and the variation of pressure as a function of height is known (Mendes, 1999). Similarly, the ZWD is a function of water vapor pressure which may be approximately described by the power law. Following Jin et al. (2007), the ZTD may be approximated as follows:

$$\text{ZTD}(h) \approx 2.277 \times 10^{(3-h/15.5)} / 0.9, \quad (4)$$

where  $h$  is the height, and the units of  $\text{ZTD}(h)$  and  $h$  are millimeter and kilometer, respectively. Eq. (4) is an approximate expression of the relationship between ZTD and height.

Accuracy of eq. (4) for describing the ZTD is assessed as ZTDs calculated from eq. (4) and that from the integrals of 313939 COSMIC occultation data in 2010 were compared. Figure 3 demonstrates that eq. (4) well expresses the ZTD's varying trend with height. Statistics suggest that eq. (4) features a bias of 9.4 cm and a standard deviation of 10.0 cm compared with the COSMIC-derived ZTD. Accuracy of eq. (4) then appears as not sufficient; however, it is not the accuracy of ZTD, but the accuracy of the variation that most applies. When height corrections are conducted, concern applies to the amount ZTD varies when the height changes  $\Delta h$ . eq. (4)'s first derivative expresses this:

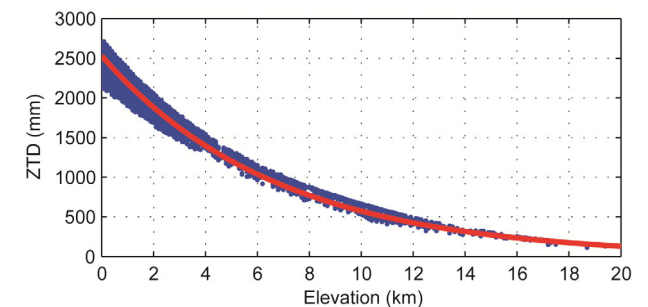


**Figure 3** Variation of ZTD with height. Red line represents ZTD calculated with eq. (4), and blue points represent ZTD derived from COSMIC occultation data.

$$\Delta\text{ZTD}(h) = -0.3758 \times 10^{(3-h/15.5)} \Delta h, \quad (5)$$

where  $\Delta\text{ZTD}$  (in mm) is the variation of ZTD as the height changes  $\Delta h$  (in km).

#### 4. Establishment of the ZTrop model

According to eq. (3), the ZTD is a function of *doy*. The annual mean ( $\alpha_1$ ) and amplitude ( $\alpha_2$ ) are both related to the

latitude and longitude.  $\alpha_1$  and  $\alpha_2$  at global grid points could be computed prior, then  $\alpha_1$  and  $\alpha_2$  in grid cells may be calculated with a bilinear interpolation. 9×9 spherical harmonics are utilized here to fit  $\alpha_1$  and  $\alpha_2$  according to the latitude and longitude as follows (Boehm et al., 2007; Yao et al., 2013):

$$\alpha_i = \sum_{n=0}^9 \sum_{m=0}^n P_{nm} (\sin \varphi) (C_{nm} \cos(m\lambda) + S_{nm} \sin(m\lambda)), \\ i = 1, 2, \quad (6)$$

where  $\varphi$  is the latitude,  $\lambda$  is the longitude,  $P_{nm}$  is the Legendre function, and  $C_{nm}$  and  $S_{nm}$  are the coefficients. Using this methods, a grid file and bilinear interpolation are possible to avoid, and only 55  $C_{nm}$  and  $S_{nm}$  (9×9 spherical harmonics have 55  $C$  and  $S$  coefficients) are essential for  $\alpha_1$  and  $\alpha_2$ , respectively. If  $P_{nm}(\sin\varphi)\cos(m\lambda)$  is replaced by  $a_p(i)$ ,  $P_{nm}(\sin\varphi)\sin(m\lambda)$  is replaced by  $b_p(i)$ ,  $C_{nm}$  is replaced by  $a_{\text{mean}}(i)$  or  $a_{\text{amp}}(i)$ , and  $S_{nm}$  is replaced by  $b_{\text{mean}}(i)$  or  $b_{\text{amp}}(i)$ , then we obtain:

$$\begin{aligned} \alpha_1 &= \sum_{i=1}^{55} [a_{\text{mean}}(i) \cdot a_p(i) + b_{\text{mean}}(i) \cdot b_p(i)], \\ \alpha_2 &= \sum_{i=1}^{55} [a_{\text{amp}}(i) \cdot a_p(i) + b_{\text{amp}}(i) \cdot b_p(i)], \end{aligned} \quad (7)$$

where  $a_{\text{mean}}(i)$ ,  $b_{\text{mean}}(i)$ ,  $a_{\text{amp}}(i)$ , and  $b_{\text{amp}}(i)$  are the unknowns as spherical harmonic coefficients, and  $a_p(i)$ ,  $b_p(i)$  are the longitude and latitude-related functions. So far, eqs. (3), (5) and (7) form the framework of our new model, and the last problem is to compute the coefficients  $a_{\text{mean}}(i)$ ,  $b_{\text{mean}}(i)$ ,  $a_{\text{amp}}(i)$ , and  $b_{\text{amp}}(i)$ .

The 5°×4° (lon×lat) GGOS ZTD data from 1st January 2008 to 31st December 2011 are applied to compute  $\alpha_1$  and  $\alpha_2$  at 3358 grid points according to eq. (3). The GGOS ZTDs are not at the same height, thus prior to calculating  $\alpha_1$  and  $\alpha_2$ , height corrections must be applied for these data. Eq. (5) is first utilized to reduce original ZTDs to ellipsoid height 0 and then, the ZTD data may be applied to compute  $\alpha_1$  and  $\alpha_2$ . The  $\alpha_1$ s and  $\alpha_2$ s are applied to compute coefficients  $a_{\text{mean}}(i)$ ,  $b_{\text{mean}}(i)$ ,  $a_{\text{amp}}(i)$ , and  $b_{\text{amp}}(i)$  according to eq. (4), yielding the ZTrop model.

The ZTrop model may be expressed by such a function, ZTD = ZTrop( $\varphi, \lambda, h, \text{doy}$ ). When the ZTrop model is applied, latitude, longitude, height of the site and the doy of observation time must be known. The model first applies eq. (7) to compute  $\alpha_1$  and  $\alpha_2$  according to the prior calculated spherical harmonics coefficients and the latitude and longitude of the site; then the model applies eq. (3) and the computed  $\alpha_1$  and  $\alpha_2$  to calculate ZTD of the site at ellipsoidal surface; finally, eq. (5) and the height parameter are employed to reduce the ZTD to the height of the site.

ZTDs from ZTrop and ZTDs utilized to establish ZTrop are compared to illustrate how the spherical harmonics fit the GGOS ZTDs. The bias and RMS errors of the model

residuals at each grid point are calculated. Figure 4 demonstrate the bias and RMS of the fitting residuals at 3358 grid points.

Figure 4(a) indicates that bias of the ZTrop model is evenly distributed on a global scale, generally between -2 and 2 cm. Some areas of the Antarctica coast and the eastern Pacific coast feature a bias with more than 6 cm, indicating eq. (3) cannot fully express the varying pattern of the ZTD in such areas and that some systematic bias is created. Bias in oceanic areas of the southern hemisphere is relatively small and also varies slightly with locations. Figure 4(b) indicates that RMS of the ZTrop model is less than 6 cm in most regions on the Earth. The ZTrop model retains stable accuracy in latitudes 60°N–60°S with a RMS of 4–6 cm, and is more accurate in the Arctic region with a RMS of approximately 3 cm. ZTrop model features large RMSs in Greenland and Antarctic regions; however, where maximal RMS is even greater than 10 cm.

Statistics of the 3358 grid points indicate that mean bias of the ZTrop model on a global scale is -0.001 mm and the mean RMS is 4.51 cm, indicating the ZTrop model was well constraint.

## 5. Comparisons between models

GGOS Atmosphere ZTD grid data, IGS ZTD products and COSMIC-derived ZTD data were utilized to evaluate the ZTrop model and other models in this section.

### 5.1 Comparison between ZTrop, UNB and EGNOS models using IGS data

The evaluation of tropospheric delay models was performed

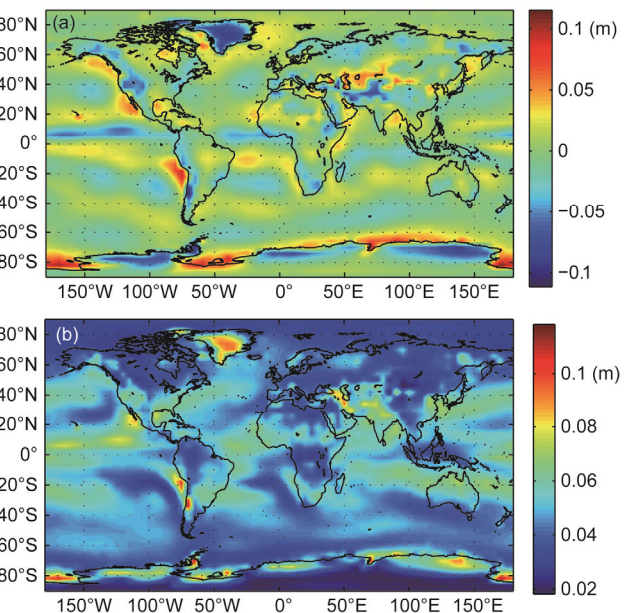


**Figure 4** Global bias (a) and RMS (b) of fitting residuals of the ZTrop model.

with the IGS ZTD products in the whole 2010. According to Byun and Bar-Sever (2009), the new troposphere ZTD products possess typical formal errors of 1.5–5 mm. Wang et al. (2007) assigned an accuracy of roughly 4 mm for the IGS ZTD products, indicating the IGS ZTD data retain reliable accuracy and are suitable to examine the ZTD from the models.

The globe was divided into  $30^\circ \times 15^\circ$  grid cells according to the longitude and latitude, with one IGS station for each grid in principle. Herein, the IGS data are considered as true values. The ZTrop model, UNB3 model, UNB3m model, UNB4 model and the EGNOS model are compared to the true values.

The IGS stations employed to evaluate models in Figure 5 are not sufficient to assess accuracy of the models as only a few are in higher locations. Comprehensive testing is ensured as 42 IGS stations at elevated heights ( $>500$  m) are added to the testing with a total of 123 IGS stations obtained. Considering the slow changes in ZTD, sampling is conducted every 3 hours, i.e. ZTD is averaged every 3 hours. Approximately 2800 ZTD values were obtained for each station in 2010.

The Mean bias and RMS error between the ZTDs derived from models and true values were computed for each site. Bias and RMS of the ZTrop model are smaller compared with other models (Figure 6). Figure 6 indicates that all models attain a greater accuracy in the northern hemisphere than in the southern hemisphere. Table 1 indicates that ZTD may be predicted within a few centimeters by the ZTrop model with a global mean bias around  $-1.0$  cm and a mean RMS close to 4.7 cm compared with IGS data. The absolute

bias of ZTrop is larger than the bias of UNB3m, and is smaller than those of UNB3, UNB4 and EGNOS. The ZTrop model, in addition, features a smaller mean RMS than the other four models.

The RMS of the ZTrop model is larger than 7 cm at 8 of the 123 IGS stations (Figure 7), while the other four models also exhibit poor accuracy at these 8 stations (UNB3 features an average RMS of 7.9 cm, UNB3, averages 7.2 cm, UNB4, averages 8.1 cm and EGNOS, averages 7.8 cm at these 8 sites. Such RMSs are obviously above the average values in Table 1).

## 5.2 Comparison between the ZTrop model and the VMF1 using GGOS data

ZTDs are applied in VMF1 in this section to test the ZTrop model in comparison with the other four models. 19131840 ZTDs on the grids in the whole 2012 were involved in testing. Mean bias and mean RMS of different models are presented in Table 2.

In Table 2, the ZTrop model displays no bias and features RMS of 4.5 cm, (in mean) approximately 38.4% more accurate than the UNB3 model, 29.7% more accurate than the UNB3m model, 40.8% more accurate than the UNB4 model and 36.6% more accurate than the EGNOS model, presenting a significant improvement. Mean bias and RMS are calculated on a global scale to illustrate the global error distribution (Figure 8).

Figure 8 demonstrates the ZTrop model features relatively good accuracy on a global scale, yet still retains large bias and RMS in some areas, especially around the eastern

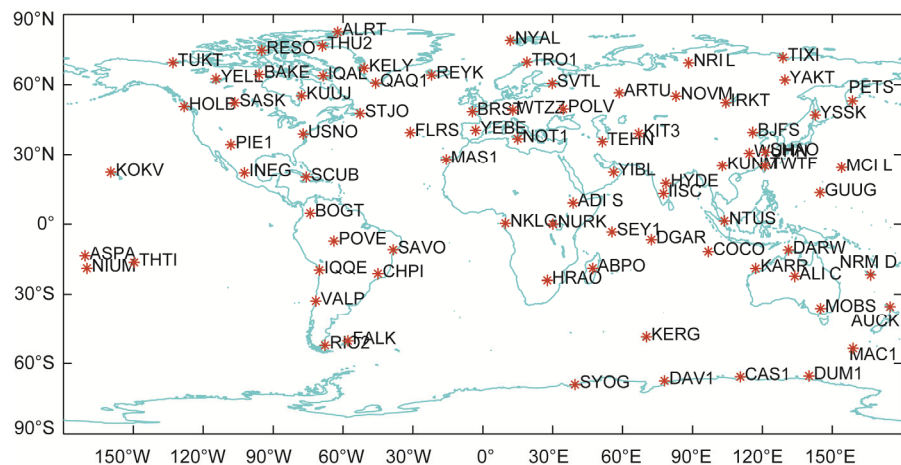


**Figure 5** Locations of IGS stations involved in the ZTrop model test.

**Table 1** Statistics of bias and RMS of the five models compared with IGS ZTD products (cm)

|      | UNB3 |      |      | UNB3m |      |      | UNB4 |      |      | EGNOS |      |      | ZTrop |      |     |
|------|------|------|------|-------|------|------|------|------|------|-------|------|------|-------|------|-----|
|      | Ave  | Min  | Max  | Ave   | Min  | Max  | Ave  | Min  | Max  | Ave   | Min  | Max  | Ave   | Min  | Max |
| Bias | 1.2  | -6.9 | 10.9 | 0.7   | -5.8 | 9.5  | 1.8  | -5.8 | 11.1 | 1.7   | -6.2 | 11.8 | -1.0  | -7.3 | 8.9 |
| RMS  | 5.5  | 3.1  | 12.4 | 5.0   | 2.5  | 10.3 | 5.6  | 3.2  | 12.6 | 5.5   | 3.5  | 12.1 | 4.7   | 2.6  | 9.5 |

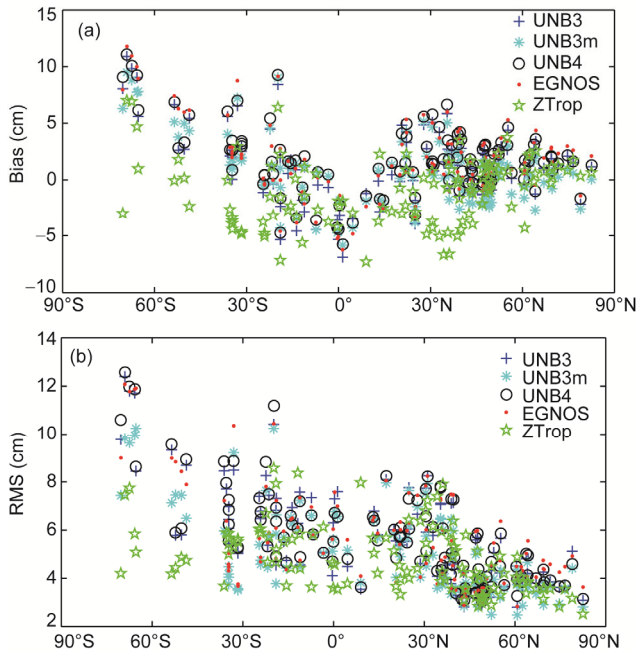


**Figure 6** Bias (a) and RMS (b) between ZTDs derived from different models and the IGS ZTDs, for each station.

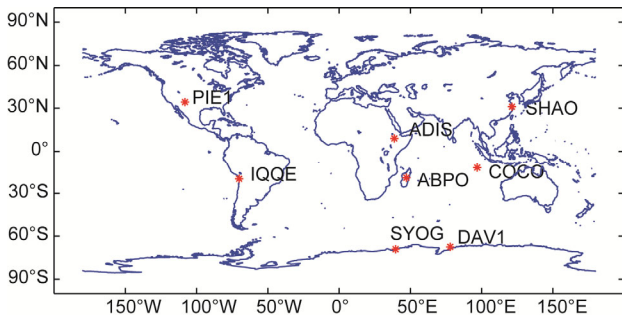


**Figure 7** 8 IGS stations where the mean RMS of the ZTrop model is larger than 7 cm.

**Table 2** Statistics of mean bias and mean RMS of the five models compared with VMF1 (unit: cm)

|           | UNB3 | UNB3m | UNB4 | EGNOS | ZTrop |
|-----------|------|-------|------|-------|-------|
| Mean bias | 4.0  | 3.3   | 4.7  | 4.5   | 0.0   |
| Mean RMS  | 7.3  | 6.4   | 7.6  | 7.1   | 4.5   |

Pacific Ocean, northern Indian Ocean and the Antarctic coast where the RMS exceeds 6 cm, aligning with previous test results in Section 5.1.

### 5.3 Comparison between models using COSMIC data

COSMIC data in 2010 were considered as true values and the mean bias and RMS difference between ZTDs derived from models and true values were computed for each latitude or longitude. Table 3 presents the global mean bias and RMS of five models. Comparing Table 2 and Table 3, re-

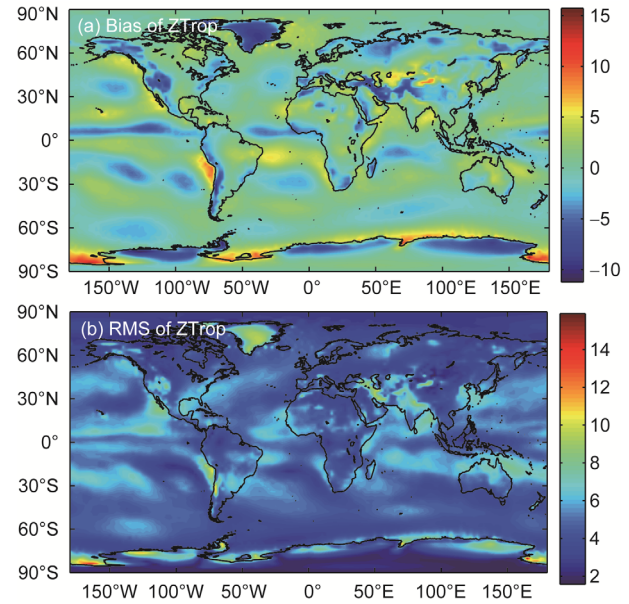


**Figure 8** Global distribution of mean bias (a) and RMS (b) between ZTDs from the ZTrop model and VMF1 data. Unit: cm

**Table 3** Statistical results of five models compared with COSMIC data on a global scale (unit: cm)

|           | UNB3 | UNB3m | UNB4 | EGNOS | ZTrop |
|-----------|------|-------|------|-------|-------|
| Mean bias | 2.4  | 2.1   | 3.0  | 3.3   | -1.3  |
| Mean RMS  | 7.1  | 6.6   | 7.3  | 7.4   | 5.2   |

sults (especially in RMS) are especially similar, as the ECMWF reanalysis data apply significant COSMIC data and the GGOS ZTD data are derived from ECMWF reanalysis data.

#### 5.3.1 The relationship between the accuracy of the models and the latitude

The globe was divided into 180 latitudinal bands with the span of each band as  $1^{\circ}$ . For each latitudinal band, the mean bias and mean RMS with respect to five models were computed (Figure 9).

Figure 9(a) illustrates that biases of the UNB3, UNB3m, UNB4 and EGNOS models are larger in the southern hemisphere than in the northern hemisphere. The four models provide annual averages and amplitudes of 5 meteorological variables between  $15^{\circ}\text{N}$  and  $75^{\circ}\text{N}$  and, when the latitude of interest is negative (in southern hemisphere), the models utilize identical meteorological variables as when latitude is positive; however, the phase is inverted (Li et al., 2012). As the four models employ the same meteorological parameter values between  $15^{\circ}\text{S}$  and  $15^{\circ}\text{N}$ , all reflect large bias in the areas. ZTrop model's performance is superior to the other four models between  $15^{\circ}\text{S}$  and  $15^{\circ}\text{N}$ ; however, large bias is also present as water vapor is abundant and changes rapidly in such areas increasing difficulty for predicting the ZWD. Poor performance of the four models south of  $40^{\circ}\text{S}$ , is likely

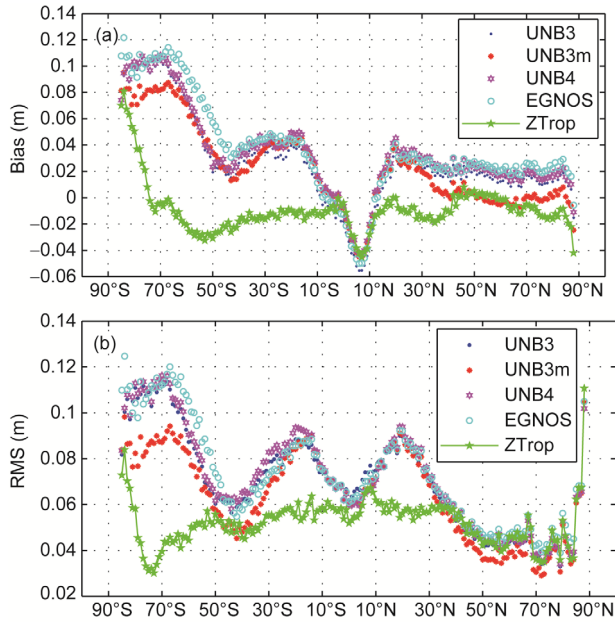


**Figure 9** Bias (a) and RMS (b) between ZTDs derived from five models and the COSMIC data, for each latitude.

attributed to the difference between the two hemispheres' climates. Performance of the ZTrop model is also compromised in Antarctic regions, likely related to extreme weath-

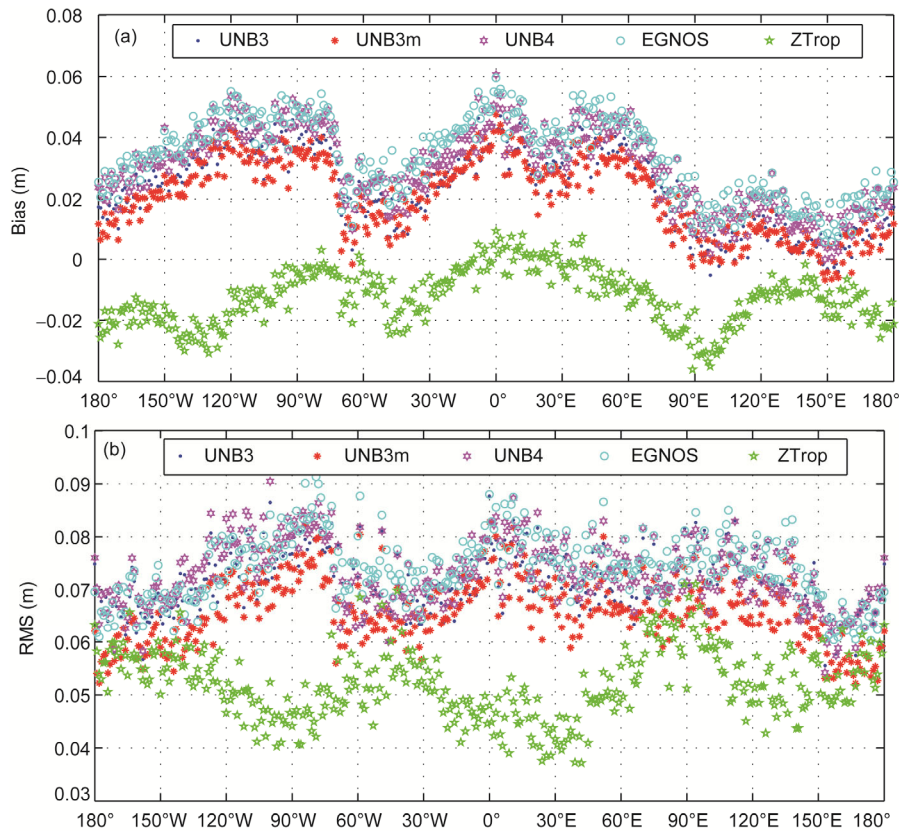
er conditions and relatively high altitudes in the region.

Figure 9(b) indicates the ZTrop model features a stable RMS below 6 cm within 80°S–80°N. The RMS of ZTrop is greater in portions of polar regions, with a maximum up to approximately 11 cm and overall accuracy of the ZTrop model remaining superior to accuracy of the other 4 models. All 4 models feature relatively large RMS (>6 cm) in areas south of 30°N due to the assumption that the southern hemisphere is a mirror of the northern hemisphere (Li et al., 2012). Compared with the ZTrop model built up with global ZTD data then, the 4 models hold distinct disadvantages.

### 5.3.2 The relationship between the accuracy of models and the longitude

The globe was divided into 360 longitudinal bands with the span of each band as 1°. Bias and RMS of five models were computed for each longitudinal band (Figure 10).

ZTrop model's performance is superior to the other 4 models (Figure 10) with UNB3m performance relatively satisfactory and EGNOS performance the least satisfactory. The bias of ZTrop is mainly below zero, fluctuating between -2 and 0 cm, while the bias of the other 4 models is positive, fluctuating between 0 and 5 cm (Figure 10(a)). RMS varies between 4 and 6 cm for the ZTrop model, and between 6 and 9 cm in the other 4 models (Figure 10(b)). Comparison between Figure 10(b) and Figure 9(b) indi-



**Figure 10** Bias (a) and RMS (b) between ZTDs derived from five models and the COSMIC-derived ZTDs for each longitude.

cates the accuracy of 5 models varies less with longitude and more with latitude. A clear correlation between accuracy of models and longitude is not apparent from Figure 10(b). As accuracy only slightly fluctuates with longitude and varying range is no more than 3 cm, likely indicating that accuracy of the models is not dependent on longitude.

#### 5.4 Comparison between ZTrop and GPT2+ Saastamoinen using IGS data

The Global Pressure and Temperature (GPT) model, based on spherical harmonics up to degree and order nine and trigonometric functions with an annual period, provides pressure and temperature at any site in the vicinity of the Earth's surface (Boehm et al. 2007). Lagler et al. (2013) published the GPT2 model by improving the spatial and temporal resolution and combining GPT and GMF (Global Mapping Function). The GPT2 model provides pressure, temperature, lapse rate, water vapor pressure, and mapping coefficients at any site, resting upon a global  $5^{\circ}$  grid of mean values, annual, and semi-annual variations in all parameters. Utilizing the meteorological parameters (mainly pressure, temperature and water vapor pressure) provided by GPT2, determination of priori ZTD by Saastamoinen model (Saastamoinen, 1972) or Hopfield model (Hopfield, 1971) is easily accomplished and acts as a conventional approach to establish tropospheric zenith delay models that emphasize modeling of meteorological parameters. While ZTrop is different from conventional models, it learns from GPT but works independently of meteorological parameters. GPT/GPT2 is superior to the meteorological parameter tables in UNB models or the EGNOS model, thus, theoretically, GPT/GPT2+Saas may provide more accurate ZTDs than UNB models and the EGNOS model. Modeling strategies in GPT/GPT2 and ZTrop are also similar, rendering a necessary comparison between GPT/GPT2+Saas and ZTrop. ZTDs from 123 IGS stations are applied as reference values to test the GPT2+Saas and ZTrop. Figure 11 illustrates the bias and RMS of each site according to latitude, and Table 4 presents statistical results of GPT2+ Saas and ZTrop.

Figure 11(a) reveals that ZTrop features more negative bias (at 75 sites) than positive bias (at 48 sites) leading to a total mean bias of  $-1.0$  cm and bias of no more than 10 cm. While the negative and positive bias of GPT2+Saas are relatively balanced (55:68), GPT2+Saas includes large bias ( $>10$  cm) at 3 sites, with the same occurrence for RMS (Figure 11(b)). Except for the 3 sites where bias and RMS are greater than 10 cm, the ZTrop and GPT2+Saas feature similar RMS at the other sites, contributing to a similar total mean RMS. Comparison in this section preliminarily demonstrates that whether modeling meteorological parameters or directly modeling the ZTD, satisfactory results may be achieved with nearly equivalent performance.

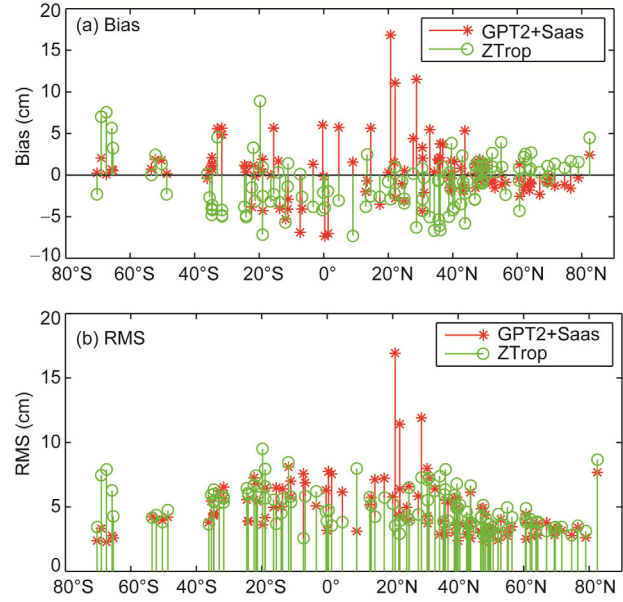


**Figure 11** Bias (a) and RMS (b) between ZTDs derived from Saas+GPT2 and ZTrop with respect to IGS ZTDs.

**Table 4** Statistical results of GPT2+ Saas and ZTrop examined by ZTDs from 123 IGS stations in 2010 (unit: cm)

|           | GPT2+Saas | ZTrop |
|-----------|-----------|-------|
| Mean Bias | 0.5       | -1.0  |
| Mean RMS  | 4.7       | 4.7   |

#### 6. Test applicability of the ZTrop model in GPS positioning

The PPP program developed by ourselves is employed to test applicability of the ZTrop model in comparison with GPT2+Saas and UNB3m. Final products of the IGS have been applied to model the satellite orbit and clock errors. The effect of the ionosphere is eliminated by the iono-free linear combination of the L1 and L2 frequencies while Kouba and Héroux (2001) is referenced for the other correction models and a sequential least square method is adopted for the adjustment. Two seasonally unique time intervals are employed to evaluate the models: a dry winter period from February 1 to February 3 and a wet summer period from August 1 to August 3 2009. The experiment is conducted as follows: (1) the PPP estimates ZWD utilizing the random walk model; zenith hydrostatic delay is provided by the Saastamoinen model; and the mapping function is Niell Mapping Function (NMF); (2) the PPP does not estimate ZWD, but utilizes the UNB3m, ZTrop or GPT2+Saas model to provide ZTD, mapping ZTD to slant tropospheric delay by NMF; (3) the mean absolute error (MAE) between the coordinates from PPP and from IGS are computed. Six day observations of 20 IGS stations are taken, while the elevation cutoff angle is set to 10 degree. Global distribu-

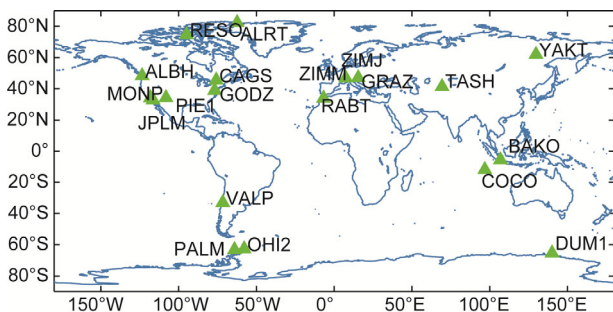
tion of 20 IGS stations is presented in Figure 12 and the MAEs of coordinates reflecting different tropospheric correction approaches are displayed in Figure 13 with statistical results listed in Table 5.

Figure 13 reveals that, for PPP, regardless of utilizing the random walk model to estimate ZWD or empirical models (ZTrop, GPT2+Saas or UNB3m) to predict ZTD, final positioning results vary little in the east and north components with most differences within 1 cm. Figure 13 also indicates the PPP features relatively large errors in up component regardless of the tropospheric correction approach utilized due to geometrical distribution of GPS satellites. Positioning error caused by tropospheric correction approaches

mainly appears in up component as the MAE of empirical models in up component is obviously larger than that of the random walk model. Statistical results in Table 5 further indicate that whether the PPP utilizes random walk or other empirical models, a significant difference in the east or north component will not occur ( $>1$  cm), and a greater difference (~30 mm) will occur in the up component. The random walk model remains the optimal strategy for tropospheric delay correction for high-precision positioning (millimeter level). Empirical models including UNB3, UNB3m, UNB4, EGNOS, as well as, ZTrop and GPT2+Saas may be applied for tropospheric delay correction for positioning of centimeter level precision or lower. If ZTDs from the ZTrop model are applied as virtual observations and the tropospheric model utilizes random walk, the PPP convergence (differences between calculated coordinates by PPP and the referenced coordinates from IGS no larger than 10 cm in the horizontal domain and 15 cm in the vertical domain) time will be reduced by 20% relative to the traditional PPP algorithm that does not utilize ZTDs from the ZTrop model as virtual observations. The experiment results further indicates high accuracy of the ZTrop model while exhibiting applicability of the ZTrop model in GPS-based PPP.

## 7. Conclusions

The  $9 \times 9$  spherical harmonics (eq. (7)) are employed to fit the annual mean and amplitude of ZTD on a global scale. The exponential function (eq. (5)) is applied for height corrections. GGOS ZTD data between 2008 and 2011 are finally utilized to compute spherical harmonic coefficients, yielding the ZTrop model. Comprehensive tests are conducted to evaluate the accuracy of the ZTrop model. The



**Figure 12** 20 IGS stations involved in the PPP experiment.

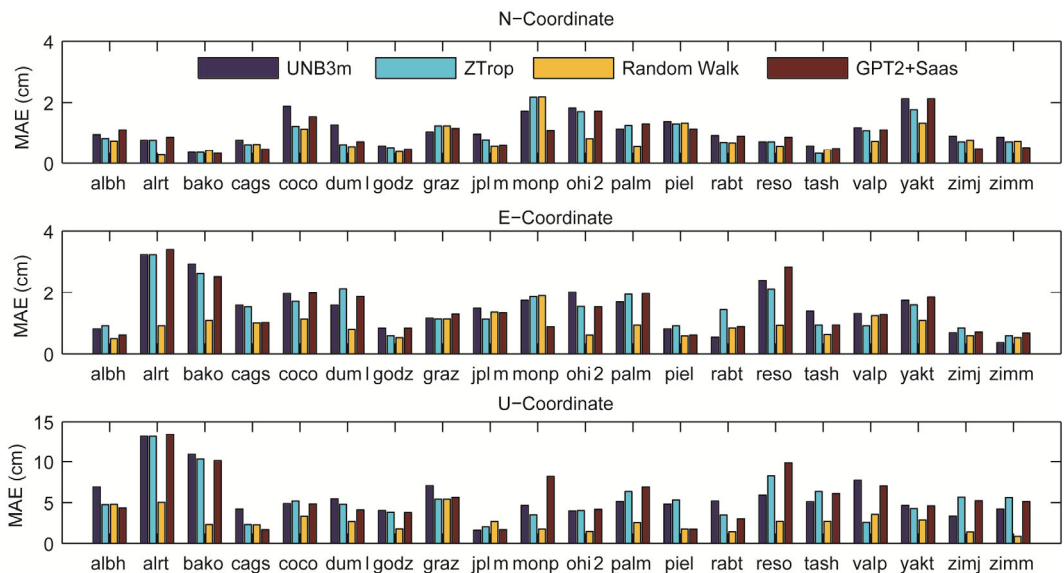


**Figure 13** Mean absolute positioning error in the north, east and up components at 20 IGS stations utilizing two different tropospheric correction approaches.

Table 5 Statistical results at 20 IGS stations utilizing two different tropospheric correction approaches in PPP solutions (mm)

|                     | Tropospheric approaches | North | East | Up   |
|---------------------|-------------------------|-------|------|------|
| Mean absolute error | Random walk             | 8.1   | 8.8  | 24.2 |
|                     | ZTrop model             | 9.7   | 14.5 | 52.1 |
|                     | GPT2+Saas               | 9.4   | 13.9 | 53.2 |
|                     | UNB3m                   | 11.0  | 14.6 | 53.8 |

ZTrop exhibits, on a global scale, an average deviation of  $-1.0\text{ cm}$  and RMS of  $4.7\text{ cm}$  compared with the IGS ZTD products, an average deviation of  $0.0\text{ cm}$  and RMS of  $4.5\text{ cm}$  compared with the GGOS ZTD data, and an average deviation of  $-1.3\text{ cm}$  and RMS of  $5.2\text{ cm}$  compared with the COSMIC ZTD data. Results for the ZTrop model are  $14.5\%$  more advanced than UNB3,  $6.0\%$  more advanced than UNB3m,  $16\%$  more advanced than UNB4,  $14.5\%$  more advanced than EGNOS and equivalent to the GPT2+Saas model for RMS in comparison with IGS data.

Applying the ZTrop, UNB3m and GTP2+Saas model to PPP in comparison with random walk, positioning results indicate that different approaches yield minimal differences in the east and north component and more significant differences ( $\sim 3\text{ cm}$ ) in up component, indicating the ZTrop model may be employed for tropospheric delay correction in GPS-based PPP of centimeter level precision or lower precision. PPP convergence time is reduced by  $20\%$  by applying ZTDs from the ZTrop model as virtual observations. The ZTrop model will then aid in cm-precision positioning by providing initial values or virtual observations of tropospheric delay, subjects intended for further research.

**Acknowledgements** The authors would like to thank the IGS, GGOS Atmosphere and COSMIC for providing the related data. This project was financially supported by the National Natural Science Foundation of China (Grant Nos. 41174012 & 41274022), the National High Technology Research and Development Program of China (Grant No. 2013AA122502), the Fundamental Research Funds for the Central Universities (Grant No. 201421402020), and the Surveying and Mapping Basic Research Program of National Administration of Surveying, Mapping and Geoinformation (Grant No. 13-02-09).

## References

- Bevis M, Businger S, Chiswell S, Herring T A, Anthes R A, Rocken C, Ware R H. 1994. GPS meteorology: Mapping zenith wet delays onto precipitable water. *J Appl Meteorol*, 33: 379–386
- Boehm J, Heinkelmann R, Schuh H. 2007. Short note: A global model of pressure and temperature for geodetic applications. *J Geod*, 81: 679–683
- Boehm J, Werl B, Schuh H. 2006. Troposphere mapping functions for GPS and very long baseline interferometry from European Centre for Medium-Range Weather Forecasts operational analysis data. *J Geophys Res*, 111, doi: 10.1029/2005JB003629
- Collins J P, Langley R B. 1997. A tropospheric delay model for the user of the Wide Area Augmentation System. Final contract report for Nav Canada, Department of Geodesy and Geomatics Engineering Technical Report No. 187, University of New Brunswick, Fredericton, N.B., Canada
- Collins J P, Langley R B, LaMance J. 1996. Limiting factors in tropospheric propagation delay error modelling for GPS airborne navigation. *Proceedings of the Institute of Navigation 52nd Annual Meeting*, Cambridge, MA, USA, 19–21 June 1996. 519–528
- Collins J P, Langley R. 1998. The residual tropospheric propagation delay: How bad can it get? 11th International Technical Meeting of the Satellite Division of the Institute of Navigation, Nashville, Tennessee. ION GPS-98. 729–738
- Davis J L, Herring T A, Shapiro I I, Rogers A E E, Elgered G. 1985. Geodesy by radio interferometry: Effects of atmospheric modeling errors on estimates of baseline length. *Radio Sci*, 20: 1593–1607
- Hopfield H S. 1971. Tropospheric effect on electromagnetically measured range: Prediction from surface weather data. *Radio Sci*, 6: 357–367
- Janes H W, Langley R B, Newby S P. 1991. Analysis of tropospheric delay prediction models: Comparisons with ray-tracing and implications for GPS relative positioning. *B Geod*, 65: 151–161
- Kouba J, Héroux P. 2001. Precise point positioning using IGS orbit and clock products. *GPS Solut*, 5: 12–28
- Lagler K, Schindelegger M, Böhm J, Krásná H, Nilsson T. 2013. GPT2: Empirical slant delay model for radio space geodetic techniques. *Geophys Res Lett*, 40: 1069–1073
- Leandro R, Santos M C, Langley R B. 2006. UNB neutral atmosphere models: Development and performance. *Proc ION NTM 2006*, January 18–20, Monterey, California, USA. 564–573
- Li W, Yuan Y B, Ou J K, Li H, Li Z. 2012. A new global zenith tropospheric delay model IGGtrop for GNSS applications. *Chin Sci Bull*, 57: 2132–2139
- Li W, Yuan Y, Ou J, Chai Y, Li Z, Liou Y, Wang N. 2015. New versions of the BDS/GNSS zenith tropospheric delay model IGGtrop. *J Geodesy*, 89: 73–80
- Mendes V. 1999. Modeling the neutral-atmospheric propagation delay in radiometric space techniques. Doctoral Dissertation. Brunswick: University of New Brunswick
- Mendes V B, Langley R B. 1999. Tropospheric zenith delay prediction accuracy for high-precision GPS positioning and navigation. *Navigation*, 46: 25–34, doi: 10.1002/j.2161-4296.1999.tb02393.x
- Niell A E. 1996. Global mapping functions for the atmosphere delay at radio wavelengths. *J Geophys Res*, 101: 3227–3245
- Jin S, Park J, Cho J, Park P. 2007. Seasonal variability of GPS-derived zenith tropospheric delay (1994–2006) and climate implications. *J Geophys Res*, 112: D09110
- Penna N, Dodson A, Chen W. 2001. Assessment of EGNOS tropospheric correction model. *J Navig*, 54: 37–55
- Saastamoinen J. 1972. Introduction to practical computation of astronomical refraction. *B Geod*, 106: 383–397
- Tuchband T. 2010. Evaluation of the EGNOS troposphere model in precise point positioning applications. *Pollack Period*, 5: 27–38
- Wang J, Zhang L, Dai A, Van Hove T, Van Baelen J. 2007. A near-global, 2-hourly data set of atmospheric precipitable water from ground-based GPS measurements. *J Geophys Res*, 112: D11107, doi: 10.1029/2006JD007529
- Webb F H. 1993. An introduction to the GIPSY/OASIS II. *JPL Publ*, D-11088
- Yao Y B, Zhang B, Yue S Q, Xu C Q, Peng W F. 2013. Global empirical model for mapping zenith wet delays onto precipitable water. *J Geod*, 87: 1–10